Geophys. J. Int. (2003) **155,** 350–366

A lock-in model for the complex Matuyama-Brunhes boundary record of the loess/palaeosol sequence at Lingtai (Central Chinese Loess Plateau)

S. Spassov,[1] F. Heller,[1] M. E. Evans,[2] L. P. Yue[3] and T. von Dobeneck[4]

[1] *Institut für Geophysik, ETH Zürich,* CH-8093 *Zürich, Switzerland. E-mail: simo.spassov@mag.ig.erdw.ethz.ch*
[2] *Institute for Geophysical Research, University of Alberta,* T6G 2J1, *Edmonton, Alberta, Canada*
[3] *Department of Geology, Northwest University,* 710 069 *Xi'an, Shaanxi Province, China*
[4] *Fachbereich Geowissenschaften, Universität Bremen, Postfach* 320440, D-283334 *Bremen, Germany*

Accepted 2003 May 1. Received 2003 March 31; in original form 2002 August 15

SUMMARY

In most marine sedimentary records, the Matuyama-Brunhes boundary (MBB) has been found in interglacial oxygen isotope stage 19. In the magnetostratigraphic records of most Chinese loess/palaeosol profiles the MBB is located in loess layer L8, which was deposited during a glacial period. The MBB at Lingtai (central Chinese Loess Plateau) also occurs in L8 and is characterized by multiple polarity flips. The natural remanent magnetization is mainly carried by two coexisting components. The higher coercivity (harder) component dominates in loess layers and is thought to be of detrital origin. The lower coercivity (softer) component prevails in palaeosols and was most probably formed *in situ* by (bio-)chemical processes. A lock-in model for the Lingtai MBB record has been developed by extending the lithologically controlled PDRM model of Bleil & von Dobeneck (1999). It assumes two lock-in zones. The NRM of the magnetically harder component is physically locked by consolidation shortly after loess deposition, whereas the softer component is formed at greater depth by pedogenesis and acquires a chemical remanent magnetization of younger age. At polarity boundaries, grains carrying reversed and normal directions may therefore occur together within a single horizon. The model uses ARM coercivity spectra to estimate the relative contributions of the two components. It is able to explain the observed rapid multiple polarity flips and low magnetization intensities as well as the stratigraphic shift of the Lingtai MBB with respect to the marine records.

Key words: chemical remanent magnetization, China, detrital remanent magnetization, loess, Matuyama-Brunhes boundary, palaeosol.

1 INTRODUCTION

The Matuyama-Brunhes boundary (MBB) has been observed in many sediment cores from different oceans. Tauxe *et al.* (1996) compiled 19 such records with sedimentation rates of up to 8 cm kyr^{-1} and confirmed that the MBB occurs in most cores in sedimentary layers representing the interglacial oxygen isotope stage 19. Astronomical calibration of the marine oxygen isotope record places the MBB at 778.8 ± 2.5 ka (Tauxe *et al.* 1996). This date agrees well with radiometric ages derived from volcanic sequences, which give 778.2 ± 3.5 ka (Tauxe *et al.* 1996) or 780 ± 10 ka (Spell & McDougall 1992) as the best estimate. Tauxe *et al.* (1996) also reported that the natural remanent magnetization (NRM) in marine sediments is fixed within a few centimetres of the water-sediment interface. Among others, deMenocal *et al.* (1990) and Bleil & von Dobeneck (1999), report downward shifts of magnetic polarity boundaries in marine sediments, with values ranging of 7 to 17 cm.

Surface layers of marine sediments are commonly unconsolidated due to high porosity and frequent bioturbation in the upper 5–15 cm. An acquired depositional remanent magnetization (DRM) cannot persist under these conditions (Guinasso & Schink 1975). According to the widely accepted concept of a post-depositional remanent magnetization (PDRM), the magnetization is gradually locked below this unstable layer after a certain amount of overburden has accumulated on the palaeosurface (Irving & Major 1964; Kent 1973; Otofuji & Sasajima 1981). Because the post-depositional fate of each magnetic particle is of a statistical nature, any magnetic assemblage will exhibit a distribution of different individual lock-in depths – even under the most idealistic assumption of uniform magnetic and non-magnetic matrix particle sizes. The macroscopic process is therefore appropriately described by a 'lock-in zone' (Løvlie

1976; Niitsuma 1977) rather than by a sharp 'lock-in front'. Consequently, lock-in not only delays remanence acquisition with regard to sediment age, but it also acts as a smoothing filter in the depth and time domains. Effects of delayed and gradual recording upon the palaeomagnetic fidelity of homogeneous sediments have been mathematically investigated by Denham & Chave (1982) and Hyodo (1984).

Bleil & von Dobeneck (1999) defined the *initial lock-in depth* d_0 as the depth above which no lasting magnetization is acquired. Under simple assumptions, a magnetic polarity boundary appears in the record where 50 per cent of the magnetic moments have been blocked parallel to the old polarity, and 50 per cent of the moments are blocked parallel to the new field polarity. The corresponding depth is called the *median lock-in depth* $d_{1/2}$. The depth where *all* available magnetic particles have been fixed is the *total* or *terminal lock-in depth* d_1.

If lock-in is regarded as a steady-state process, brief polarity intervals will be recorded only if they last longer than the median lock-in depth divided by the sedimentation rate. Therefore, short-lived geomagnetic events may not impart a clear polarity imprint on a PDRM record.

Terrestrial loess sediments also record geomagnetic field behaviour. Loess sequences consist of loess/palaeosol alternations where loess layers are relatively fresh aeolian deposits formed during colder climate periods, whereas palaeosols develop on a loess layer by pedogenic processes during warmer and wetter conditions. Heller & Liu (1982, 1984) observed the MBB at Luochuan (central Chinese Loess Plateau, CLP) in the 8th palaeosol (palaeosol S8) from the top of the sequence. Many other authors observed this boundary in the more recently deposited loess layer above S8 (called L8 according to the nomenclature of Liu & Chang 1964). Sometimes the MBB was not noticed at all in this entire stratigraphic interval (Hus & Han 1992). Hus & Han (1992) pointed out that different PDRM lock-in depths could explain the different stratigraphic positions of the MBB. There is now overwhelming evidence that the MBB on the Chinese Loess Plateau is recorded mostly in loess layer L8 (Liu *et al.* 1988; Cao *et al.* 1988; Rolph *et al.* 1989; Rutter *et al.* 1990; Zheng *et al.* 1992; Li *et al.* 1997; Ding *et al.* 1998; Zhu *et al.* 1998; Spassov *et al.* 2001).

Variability of lock-in depths may be due to different post-depositional processes. The fixing of magnetic grains in loess depends on the stabilization of the sediment microstructure. After the settling of the dust particles, 'loessification' (transformation of dust into loess coupled with secondary calcification) establishes this microstructure. This structural change takes place in a depth zone between $\sim$0.4 and $<$1 m under specific loading and wetting conditions (Assallay *et al.* 1998). In addition, the presence of oxidized titanomagnetites (Heller & Liu 1984), the alteration of unstable minerals (biotite, augite) in strongly weathered loesses (Liu 1985) and the reductive dissolution of iron which can be reprecipitated in oxidizing or carbonate-rich environments (Perel'man 1977) would also argue for the formation of a chemical or crystallization remanent magnetization (CRM).

Based on a detailed stratigraphic comparison between neighbouring loess/palaeosol sections of the central CLP, Heller *et al.* (1987) suggested local relative remanence lock-in delays of about 20 kyr for the MBB and proposed a correlation of palaeosol S7 with marine oxygen isotope stage 19. Zhou & Shackleton (1999) compared the MBB records of deep-sea cores and other (lacustrine) continental sediments and concluded that the MBB should be observed within oxygen isotope stage 19. They considered the MBB position in the marine sediments as a reliable time marker and argued that the MBB in the loess sediments at Luochuan, the classical section on the CLP, was displaced downward by 1.7 to 2.5 m and that oxygen isotope stage 19 should be correlated with palaeosol S7. They used the 700–800 ka old Australasian micro tektite layer, which was observed in deep-sea cores about 12 kyr before the MBB (Schneider *et al.* 1992; Kent & Schneider 1995), to fix their correlation in an absolute time frame. Some microtektites have also been identified in the upper part of L8, but above the recorded MBB (Li *et al.* 1993).

The Chinese loess/palaeosol timescale developed by Heslop *et al.* (2000) is based on the correlation of astronomically tuned monsoon records with the oxygen isotope record of ODP site 677 (Shackleton *et al.* 1990). Heslop *et al.* (2000) concluded that the polarity boundaries are displaced and shifted downward in the loess stratigraphy. They arrived at shift estimates of 1.90 m at Baoji (central CLP) and 1.59 m at Luochuan, which would correspond to time delays of 26 and 23 kyr, respectively, and they also suggested a correlation of palaeosol S7 with marine oxygen isotope stage 19 (see also Evans & Heller 2001).

The present study is intended to shed some light on the processes, which cause the apparent time lag of the MBB in the Chinese loess sediments with respect to the marine record. The loess section at Lingtai (central CLP) has been selected for detailed rock- and palaeomagnetic measurements. Post-depositional and chemical processes of remanent magnetization acquisition will be considered in the development of a lock-in model, which extends the PDRM model proposed by Bleil & von Dobeneck (1999).

2 MAGNETIC POLARITY BOUNDARIES AND ROCK MAGNETIC PROPERTIES OF THE LINGTAI SECTION

The Lingtai section (107.56°E, 34.98°N) is located in the central part of the CLP. The upper 175 m of the 305-m-thick section consists of alternating loess/palaeosol and the lower part is formed by Mio-/Pliocene red clay with a basal age of about 7.05 Ma (Ding *et al.* 1998). Some 32 palaeosols have been identified in the Lingtai sequence. They can be correlated with other sections, for instance with Baoji (Rutter *et al.* 1991), and provide a complete stratigraphic sequence. The Lingtai section was sampled continuously from 0 to 268.12 m, resulting in about 13, 400 oriented cubic samples with an edge of 2 cm.

Here we discuss results from samples spanning the MBB. A first sample set (set A) was collected to provide continuous data for a 3 m stratigraphic interval from S8 through the slightly weathered L8 up to S7. All samples from set A were stepwise thermally demagnetized. Another independent sample set (set Y, collected about 1 m away from set A) was treated using alternating fields (AF) demagnetization. A secondary present-day overprint was removed at temperatures between 250°C and 300°C or at peak fields of 15 mT or 20 mT in both loess and palaeosol samples. After demagnetization treatment the MBB was found between 61.4 and 62.0 m in L8 (Fig. 1), implying an average sedimentation rate of 7.9 cm kyr^{-1} for the Brunhes part of the section.

The stable, characteristic remanent magnetization (ChRM) records seven full polarity changes at the MBB throughout a transitional zone of about 0.4 m thickness. They occur at slightly different depths in the two data sets (Fig. 1). Two intermediate VGP positions are observed in the Y data (AF) within 0.5 m below the lowermost full reversal. They are not present in set A (thermal). The partly dissimilar ChRM directions seem to reflect different demagnetization response of the coercivity and the blocking temperature distributions of the magnetic mineral fractions present.

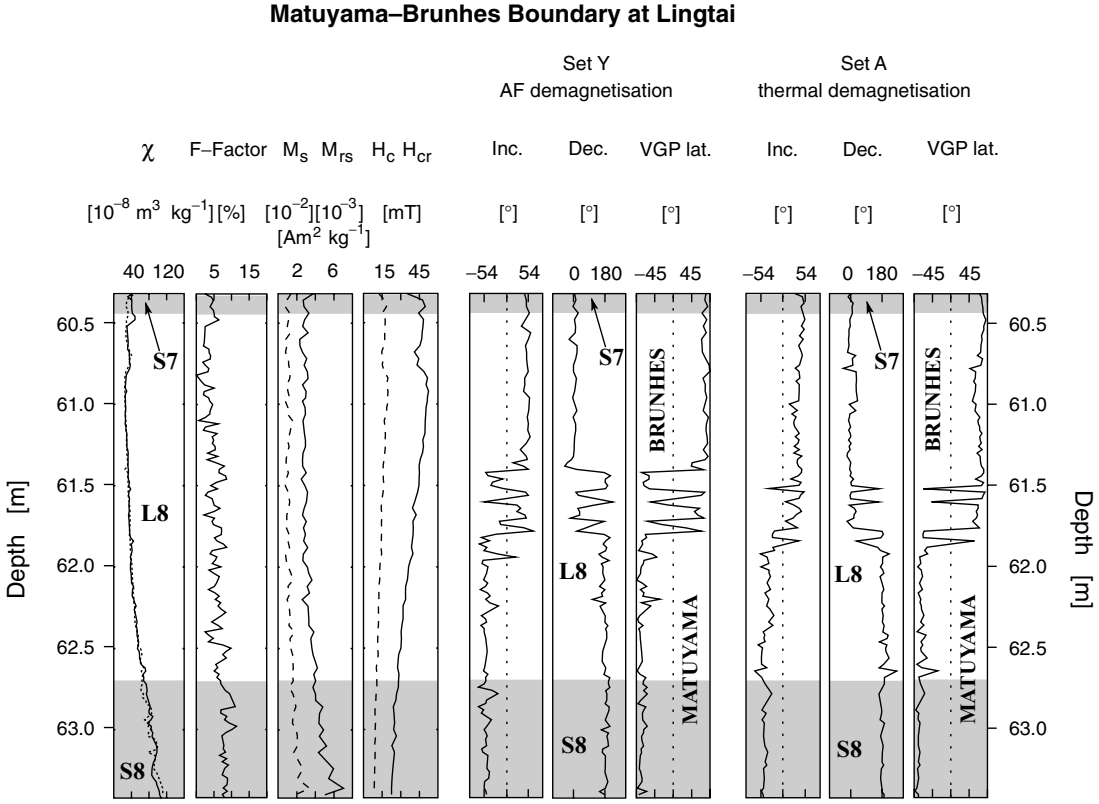

Figure 1. Continuous magnetic records across the MBB boundary at Lingtai (central CLP). The directional behaviour of the MBB transitional polarity interval (given by ChRM declination, inclination (local geocentric axial dipole inclination = 54°) and VGP latitudes, respectively) is characterized by seven full polarity changes in both data sets. Two intermediate VGP positions are located at depths 61.94 m and 62.20 m in set Y. A slight stratigraphic shift of the transitional directions is seen between thermally and AF demagnetized data. Low field susceptibility (χ), frequency dependence of susceptibility (F-factor resulting from measurements at two frequencies, 0.47 kHz and 4.7 kHz), coercivity H_c (dotted line), coercivity of remanence H_{cr} (solid line), saturation magnetization M_s (maximum field of 300 mT; dotted line) and saturation remanence M_{rs} (solid line). All rock magnetic data are from set Y, except the dotted susceptibility curve, which is from set A. Since both susceptibility curves coincide, stratigraphic consistency of both sample sets is demonstrated.

In order to assess the reliability of the data, the maximum angular deviation (MAD) of the regression line of the ChRM was calculated, using the same number of demagnetization steps (6) for all samples (Spassov *et al.* 2001). Both demagnetization methods yield approximately the same precision above and below the transition zone with MADs generally $<10^\circ$ whereas the ChRM directions are less well defined within this zone, with MADs sometimes exceeding 30°. This may be due to increasingly mixed ChRM polarity within these samples. The two intermediate VGPs also have high MAD values (Spassov *et al.* 2001).

Specific low-field susceptibility χ, coercivity H_c, coercivity of remanence H_{cr}, saturation magnetization M_s and saturation remanence M_{rs} vary smoothly across this stratigraphic section and do not show any abrupt changes near, or within, the transition interval (Fig. 1). The coercivity values slightly increase from S8 to L8 and suggest that two coercivity populations, coexist in the loess/palaeosol samples (*cf.* Evans & Heller 1994). Higher concentrations of a rather fine-grained mineral fraction (magnetite) are indicated in palaeosol S8 by higher frequency dependence of susceptibility (F-factors) and saturation magnetizations together with lower coercivities. We argue that the multiple polarity changes, which do not occur completely simultaneously in both data sets, were caused by lock-in effects rather than by geomagnetic field behaviour (see Spassov *et al.* 2001). They are not correlated with any distinct changes of the rock magnetic signature or lithology. The syn- or post-sedimentary formation of detrital and pedogenic minerals, respectively, may have had an important influence on the lock-in process of the ChRM.

3 IRM ANALYSIS

Detailed analysis of acquisition and demagnetization of isothermal remanent magnetization (IRM) data can provide critical information about coercivity distributions and related mineral phases (Robertson & France 1994; Kruiver *et al.* 2001; Egli 2003). Five samples were selected to investigate the influence of weathering and pedogenesis on the magnetic mineralogy of the loess samples using the technique of Egli (2003). The first sample (BY055) is from the L4 (depth = 69 m) of the high sedimentation rate Baicaoyuan section in the western CLP. It has a low susceptibility of 38×10^{-8} m^3 kg^{-1} and is regarded as being essentially unaltered and unaffected by weathering (see Evans & Heller 1994). The second sample (A1515, depth = 30.3 m) originates from L4 of the Lingtai section. Although this sample is from the central CLP, where sedimentation rates were lower and weathering and pedogenic alteration is generally stronger, it has an even lower susceptibility of only 21×10^{-8} m^3 kg^{-1}. The third sample (Y0030) is from the upper part of L8 (depth = 60.9 m) at Lingtai and has a susceptibility of 26×10^{-8} m^3 kg^{-1}. The most mature stage of pedogenesis within the interval of interest is expected to be seen at Lingtai in sample A2980 from the weakly developed palaeosol S7 (depth = 59.6 m). Its susceptibility is 77×10^{-8} m^3 kg^{-1}. Sample A0494 originates from one of the most

strongly developed palaeosols at Lingtai–palaeosol S1 (depth 9.88 m). It has a susceptibility of 215×10^{-8} m^3 kg^{-1}.

Preliminary IRM acquisition curves up to 4600 mT saturate at about 3000 mT for loess samples and at 1500 mT for palaeosols. Since the experiments described below involved IRM's acquired in fields up to 300 mT we will be concerned only with the low coercivity mineral content. This seems to be acceptable as the increase of the IRM acquisition curve above 300 mT is small in both lithologies. In palaeosol and loess samples 93 per cent and 85 per cent of the saturation remanence are reached at 300 mT, respectively.

All samples were first demagnetized using an AF of 300 mT along three orthogonal axes. The samples were then magnetized with a DC field of 300 mT along one axis. Tests on samples with different amounts of viscous remanence carriers show that after a waiting time of about 3 min almost no decay of the IRM was observed within the time required for the measurement to be completed. After this delay, stepwise AF demagnetization (logarithmic steps up to 300 mT) of the IRM was performed along the magnetized axis was started and the remaining IRM was measured using a 2G Enterprises cryogenic magnetometer with an in-line AF demagnetization coil. The differential IRM demagnetization curve was calculated using the following steps. First, the original curve was scaled resulting in a linear demagnetization curve. Next, the scaled demagnetization curve was fitted with a hyperbolic tangent function. Then the residuals between the fit and the data were low-pass filtered (using the same Butterworth filter parameters (order 8) for all demagnetization curves) in order to eliminate experimental noise. After backward transformation, a noise-free IRM demagnetization curve was obtained. This curve was then scaled using a logarithmic field scale (base 10), thus the field axis becomes unitless. The resulting derivative, also called the logarithmic coercivity spectrum (LCS), therefore has the same units as the magnetization (for a complete description of the method see Egli 2003).

The initial IRM demagnetization curves show progressively higher intensities with increasing degree of weathering (Figs 2a and b). All IRM gradient curves exhibit a coercivity component that peaks between 40 and 58 mT, which is attributed to minerals of detrital origin (Figs 2c and d). A lower coercivity maximum develops

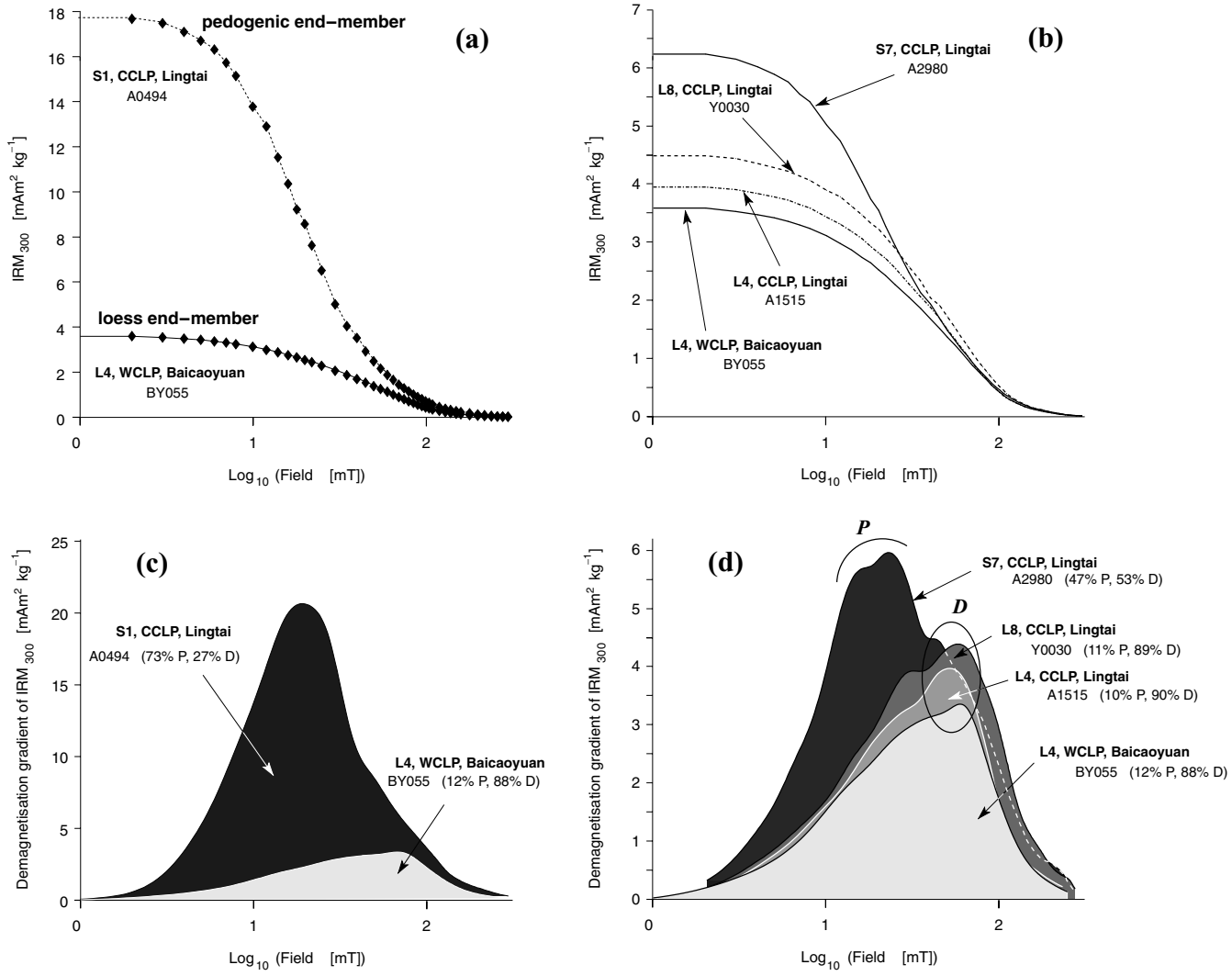

Figure 2. (a/b) AF demagnetization of IRM given at 300 mT for different loess/palaeosol samples. (c/d) Gradients of the demagnetization curves. The higher coercivity component (maximum 40–58 mT) is present in all samples (even in the strongly developed palaeosol S1) and represents the detrital population D, assumed to be uniform across the Chinese Loess Plateau (Evans & Heller 1994). With increasing humidity the loess is affected by weathering and a new low coercivity population *P* of (bio)chemical grains is formed. The contribution of each component is given in Table 1. The dashed line in (d) represents the continuation of the spectrum of palaeosol S7.

Table 1. Isolation of magnetic populations for loess/palaeosol samples.

Sample	Horizon	Location on CLP	Contribution of		Modelled initial IRM $mAm^2\ kg^{-1}$	Measured initial IRM $mAm^2\ kg^{-1}$
			P [$mAm^2\ kg^{-1}$]	D [$mAm^2\ kg^{-1}$]		
BY055	L4	western	0.43 (11.5 per cent)	3.27 (88.5 per cent)	3.70	3.63
A1515	L4	central	0.40 (9.8 per cent)	3.67 (90.2 per cent)	4.07	3.99
Y0030	L8	central	0.52 (11.2 per cent)	4.12 (88.8 per cent)	4.64	4.53
A2980	S7	central	2.94 (47.1 per cent)	3.30 (52.9 per cent)	6.24	6.25
A0494	S1	central	12.77 (72.6 per cent)	4.81 (27.4 per cent)	17.58	17.86

The pedogenic component P increases gradually from the relatively unaltered loess BY055 on the western CLP representing cold/arid climate conditions to the altered loess Y0030 on the central CLP where more humid climate conditions prevailed. Maximum pedogenesis within the interval of interest is reached in the palaeosol sample A2980.

progressively from L4 at Baicaoyuan (BY055) to L8 at Lingtai (Y0030) into the palaeosols S7 and S1. The low coercivity peak is located between 16 and 25 mT. This peak appears to be caused by pedogenic processes as demonstrated by its dominance in the spectra from palaeosols S7 and S1. The higher coercivity component of S7 (dashed line in Fig. 2d) has essentially the same amplitude as that of the parent material in L8.

The different magnetization contributions were quantified following the unmixing method proposed by Egli (2003). Magnetizations of mixed components add linearly (Stacey 1963; Kneller & Luborsky 1963; Roberts *et al.* 1995; Carter-Stiglitz *et al.* 2001). Therefore the model attributes the coercivity spectra to a number of distinct coercivity populations. Our analysis indicates the presence of one detrital (D) and one pedogenic (P) mineral population. The spectrum for sample BY055 (supposed to represent the pristine loess end-member, see Fig. 2) was subtracted from the spectrum of palaeosol S1 (supposed to represent the pedogenic end-member, see Fig. 2) in order to obtain the pedogenic component P in the sense: $P = S1 - n\cdot$ BY055 ($n = 1.5$. With this factor, the detrital component disappears completely in the spectrum of S1). After fitting P with a log-normal function, it was subtracted again from BY055 to obtain the pure detrital component: $D =$ BY055 $- k \cdot P$ ($k = 0.04$. With this factor the pedogenic component disappears in the spectrum of BY055). D was then fitted with log-normal functions. This algorithm was iteratively applied and a stable solution was reached after the second iteration step. Each pilot sample could be modelled using a linear combination of the two components. The area under each gradient curve represents its contribution to the total IRM of the sample. The percentage of the contribution was then obtained by integration of each individual component.

Whereas the detrital component is roughly constant, component P steadily increases from the almost unweathered loess BY055 and peaks in palaeosol S1 where pedogenic minerals show highest concentrations (Table 1). Thus, the contribution of population P varies depending on the stage of pedogenesis. It can also be concluded that the detrital component D is not much influenced by pedogenesis because its contribution in L8 and S7 is nearly equal. As fields up to 300 mT were applied, high coercivity minerals such as hematite or goethite contribute very little to the IRM gradient. The detrital population D (coercivity maximum between 40 and 58 mT) is interpreted as maghemite or titanomagnetite (*cf.* Eyre 1996), whereas the population P (coercivity between 16 and 25 mT) probably consists of magnetite of chemical or biochemical origin. Referring to magnetite coercivities measured on IRM acquisition curves (Maher 1988), the coercivity values for P are close to the magnetite single-domain/superparamagnetic boundary and single domain state, respectively. These attributes have to be considered with caution since AF demagnetization of IRM and DC acquisition of IRM are physically different processes and hence result in different coercivity values (Cisowski 1981; Fabian & von Dobeneck 1997; Dunlop & Özdemir 1997).

The IRM results confirm our initial assumptions about the degree of weathering of the different samples. The least altered loess sample (BY055) exhibits essentially no low coercivity peak P, but P is evident in loess Y0030 due to weathering, i.e. increasing pedogenesis. The result of our rock magnetic investigation is in agreement with the results of Sartori (2000) concerning general grain size populations, which indicate preferential formation of small grains (clay size) during pedogenesis. Because the pedogenic magnetic component was formed by chemical diagenesis, it is likely to carry a CRM, which may have been acquired under conditions different to those of the detrital component.

4 LOCK-IN MODELS

4.1 The linear detrital-pedogenic lock-in model

The principles of delayed remanence acquisition have already been discussed, experimentally tested and modelled by Løvlie (1974, 1976), Guinasso & Schink (1975), Denham & Chave (1982), Hyodo (1984), Mazaud (1996) and Meynadier & Valet (1996). Recently, a delayed remanence acquisition model was re-designed and applied to Quarternary deep-sea sediments by Bleil & von Dobeneck (1999). To summarize briefly, a layer, which is now at depth z, was progressively buried under a sediment cover of thickness ζ. During burial the magnetizations of oriented magnetic particles are gradually locked-in. The fraction of the locked magnetic moment can be described by a linear (or, alternatively, curvilinear) lock-in function λ, which depends on burial depth and the lithology.

Since loess L8 at Lingtai contains both detrital and pedogenic magnetic minerals, a new approach to the lock-in problem is required. Two remanence acquisition processes are incorporated in the definition of the lock-in function λ (Fig. 3). Below a certain depth of loess sedimentation (d_0), the detrital population starts blocking with a certain lock-in rate. The PDRM is blocked entirely at depth d_1. Meanwhile chemical weathering begins and produces a new secondary magnetic mineral population, which starts to acquire a CRM at d_2. The second lock-in phase is due to the chemical remanent magnetization (CRM), which is completed at d_3. The lock-in rate for both processes may be different. The corresponding two-stage lock-in function λ can be expressed in the following way:

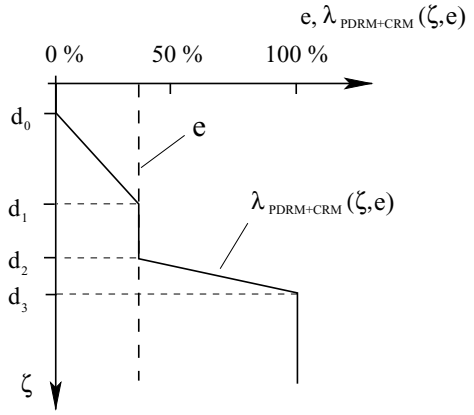

—— lock−in function, percentage of locked material $\lambda_{PDRM+CRM}(\zeta,e)$
– – – percentage of the detrital component e

Figure 3. General lock-in function $\lambda_{PDRM+CRM}(\zeta, e)$ at a given percentage of the detrital component (e) for the detrital-pedogenic remanence model, which assumes that loess is being deposited and subsequently altered. Until the initial lock-in depth d_0 is reached, no magnetization is acquired. The PDRM in the loess is locked completely after d_1 has been passed. The loess alteration may have started in the meantime and new magnetic minerals can acquire a CRM at d_2. The CRM is totally locked at d_3.

$$\lambda_{PDRM+CRM} = \lambda(\zeta, e(z)) = \begin{cases} 0 & \text{for} \quad \zeta < d_0 \\ e(z)\dfrac{\zeta - d_0}{d_1 - d_0} & \text{for} \quad d_0 \le \zeta < d_1 \\ e(z) & \text{for} \quad d_1 \le \zeta < d_2 \\ e(z) + (1 - e(z))\dfrac{\zeta - d_2}{d_3 - d_2} & \text{for} \quad d_2 \le \zeta < d_3 \\ 1 & \text{for} \quad \zeta \ge d_3. \end{cases} \tag{4.1}$$

Note that the depth ranges of the two lock-in zones for PDRM and CRM are taken as constants throughout the model space. The newly introduced PDRM/CRM ratio $e(z)$ which describes lithogenic change, quantifies the relative contribution of the PDRM (loess) fraction to the total NRM. Accordingly, $100-e(z)$ represents the NRM percentage that is due CRM (palaeosol). The coefficient $e(z)$ can vary between 0 and 100 per cent, i.e. between the two theoretical lock-in model end-members of 'pure loess' and 'pure palaeosol'. A sketch of the two-component lock-in process during a geomagnetic field reversal is given in Fig. 4. The remanence contribution of each lock-in zone to the total remanence depends on the variation of e with depth.

When modelling the lock-in process (see Fig. 4), burial depth ζ is incremented in discrete steps $i = 1...n$. The incremental magnetization from ζ_{i-1} to ζ_i acquired at the present z is proportional to the increment of the linear lock-in function $\Delta\lambda = \lambda[\zeta_i, e(z)] - \lambda[\zeta_{i-1}, e(z)]$ called the lock-in rate. $\mathbf{H}(z)$ is the intensity of the local magnetic field at the time when the layer at z was deposited. Only two antiparallel field directions (normal and reversed) are assumed and introduced as positive and negative values of $\mathbf{H}(z)$, respectively. The average magnetic field over the interval is $\frac{1}{2}[\mathbf{H}(z-\zeta_i)+\mathbf{H}(z-\zeta_{i-1})]$. The total remanent magnetization $\mathbf{M}$ is obtained by multiplying both terms and by summing up the partial remanences (arrows in Fig. 4) of all n steps to $\zeta_n = z$:

$$\mathbf{M}(z) = \sum_{i=1}^{n} \{\lambda_{PDRM+CRM}[\zeta_i, e(z)] - \lambda_{PDRM+CRM}[\zeta_{i-1}, e(z)]\} \cdot \frac{\mathbf{H}(z-\zeta_i) + \mathbf{H}(z-\zeta_{i-1})}{2}. \tag{4.2}$$

This equation can be written in analytical form:

$$\mathbf{M}(z) = \int_{\zeta=0}^{z} \frac{\partial \lambda_{PDRM+CRM}(\zeta, e(z))}{\partial \zeta} \mathbf{H}(z-\zeta)\, d\zeta. \tag{4.3}$$

The strength of the reversing geomagnetic magnetic field $\boldsymbol{H}$ will be simulated by a hyperbolic tangent function ranging from −1 to 1:

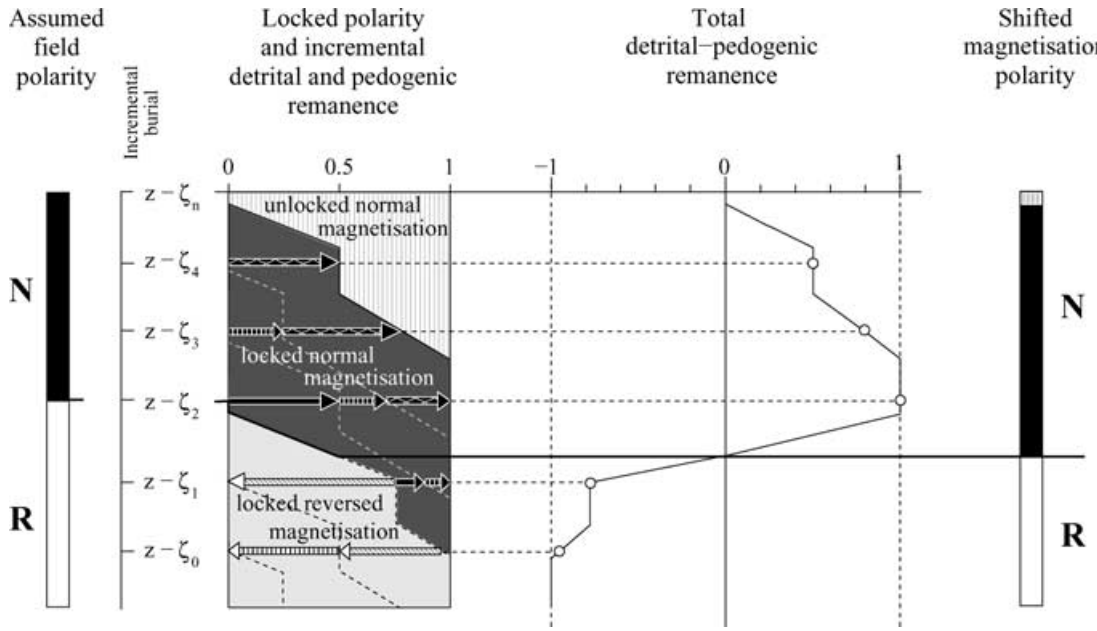

Figure 4. Schematic lock-in process of a two-component (detrital and pedogenic) remanence during a field reversal. The remanence is composed of contributions (arrows) from different discrete lock-in zones separated by the lock-in isochrons (dashed). Equally shaded arrows indicate their affiliation to the respective lock-in zone. A change in magnetic polarity will be observed when more than half of the total magnetic moments are blocked in the new field direction.

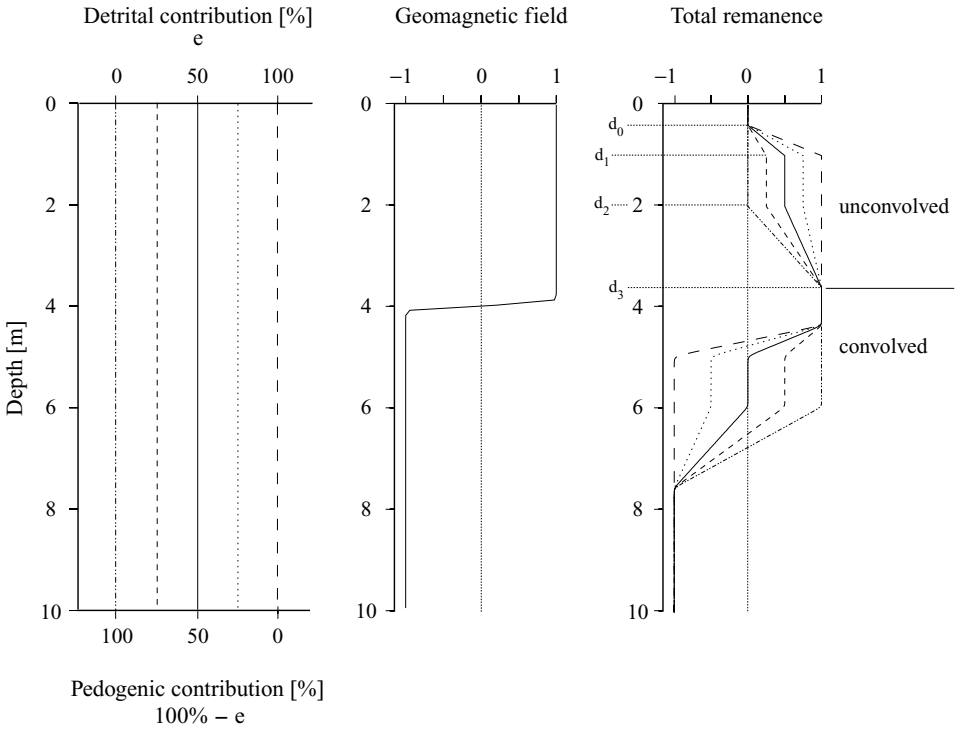

Figure 5. Modelled detrital-pedogenic remanence for different constant detrital contributions. Left: The detrital contribution is constant over the whole model space at five different values (0, 25, 50, 75, 100 per cent). Middle: A geomagnetic field reversal is modelled as a tanh function centred at 4 m depth. Right: The modelled remanence acquisition is divided into two parts. The part from 0 to about 3.5 m describes the lock-in process from the surface. Since the field polarity does not change during this most recent lock-in, the lock-in function is not convolved with the derivative of the geomagnetic field. This part of the remanence simply reflects the lock-in function (first term of eq. 4.6). If the polarity of the field changes during lock-in, the lock-in function is convolved with the derivative of the field. Therefore a distorted image of the lock-in process is obtained (it is convolved). The value of the plateau near 5–6 m depends on the lithogenic ratio e. Small lithogenic variations can easily cause multiple polarity flips of the magnetization, if both mineral components (detrital and chemical) are nearly equally represented.

$$\boldsymbol{H}(z) = -\tanh\left[\frac{c_2 + c_1}{c_2 - c_1}\left(z - \frac{c_2 + c_1}{2}\right)\right]. \tag{4.4}$$

The constants c_1 and c_2 represent the end and the beginning of the reversal, respectively. The application of the linear detrital-pedogenic lock-in model to different artificial PDRM/CRM ratios is shown in Fig. 5, $e(z)$ being assumed constant. Nearly equal contributions of PDRM and CRM constitute an extremely sensitive balance for polarity changes and result easily in recording of multiple polarity flips despite a simple step-function reversal.

The model relies on the following assumptions: Each magnetic grain is either locked or free to align its magnetic moment parallel to the external field. The dependence on field strength has not been considered because relevant experimental data are missing. The lock-in function λ depends only on lithology $e(z)$ and burial depth ζ. The lock-in rate for each process is constant (linear model).

4.1.1 Estimation of the model parameters

The model assumes that detrital lock-in starts when a loess layer of thickness d_0 has accumulated. This may be due to 'loessification' which is known to take place between about 0.4 and 1 m (Assallay *et al.* 1998); these two values are taken to be appropriate estimates for d_0 and d_1, respectively. It is assumed that pedogenic remanence carriers may start precipitating already during loess deposition. A pedogenic CRM in those mineral phases may begin blocking shortly after the detrital population has been locked. A small depth difference between d_1 and d_2 of only 0.20 m was chosen at first, corresponding to a time interval of ~2500 yr and a value of 1.2 m for d_2. A value of 3.2 m was found to be appropriate for d_3. This lock-in depth corresponds to half of the MBB shift on the CLP (see Heslop *et al.* 2000; Zhou & Shackleton 1999).

The function $e(z)$ was estimated from detailed anhysteretic remanent magnetization (ARM) measurements. The ARM is supposed to respond to the mineral populations that carry the detrital and pedogenic NRM components. When an ARM (maximum AF of 150 mT, DC bias field of 0.05 mT) was subjected to stepwise AF demagnetization, different lithologies were found to exhibit two distinct coercivity populations (Fig. 6). The derivative of the demagnetization curve of palaeosol S1 is dominated by a single maximum located at 21 mT, whereas the pristine loess L4 has a major peak at 44 mT in addition to the much less developed pedogenic component. The maxima of the gradient curves of ten previously investigated samples (not shown here) vary within intervals of 1.3 mT and 1.5 mT for the low and high coercivity samples, respectively. This method therefore provides robust estimates of the lithogenic ratio function $e(z)$. For the 137 samples at Lingtai between depths of 60.32 and 63.38 m, we chose the central difference quotients (typically on the order of 10^{-6} A m^{-1} mT^{-1}) around the two peak values as a measure of the contribution of detrital and pedogenic components. The lithogenic ratio was then calculated as:

$$e(z) = \frac{\Delta ARM_{44mT}(z)}{\Delta ARM_{21mT}(z)} \cdot 100\,\text{per cent}. \tag{4.5}$$

Repeat measurements of selected samples indicate that the error in $e(z)$ is between 1 and 3 per cent.

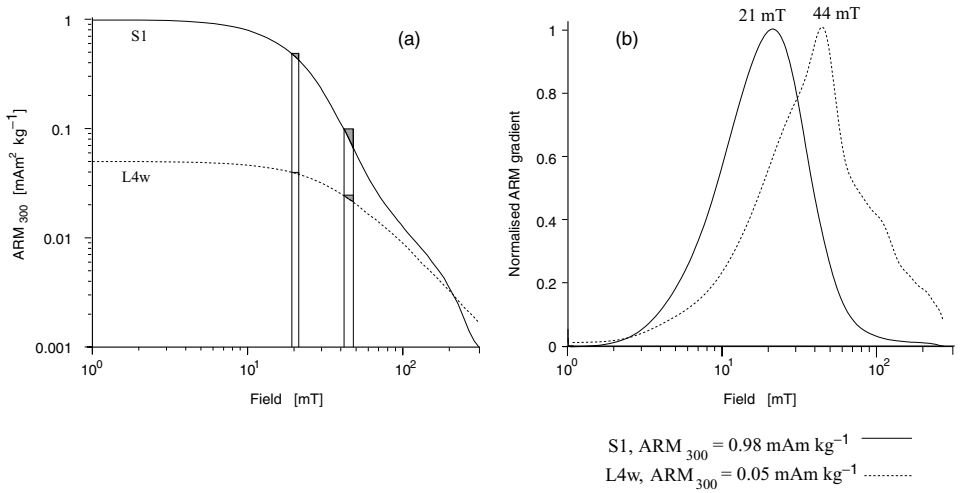

Figure 6. ARM demagnetization curves and ARM coercivity spectra of two samples with different lithogenic properties. Sample S1 is from Lingtai and represents the pedogenic end-member. Sample L4w is from L4 in the Baicaoyuan section (Evans & Heller 1994), western CLP, and is regarded as the unweathered loess end-member. (a) In order to calculate the lithogenic ratio e, the central difference quotients at 21 and 44 mT were chosen to represent the pedogenic and detrital remanences, respectively. (b) The ARM coercivity spectra for the end-members clearly show two separate peaks.

4.1.2 Sensitivity test

Before applying the detrital-pedogenic model to the loess/palaeosol sediments of Lingtai using the measured ARM properties, it was first tested using arbitrary $e(z)$ functions. The lithogenic ratio was assumed to vary sinusoidally between 0 and 100 per cent every 0.2 m over a model space of 8 m. A field change from reversed to normal polarity is supposed to start at 4.15 m and to last for 0.4 m.

First the lock-in function is depicted at a level where sedimentation has stopped at 0 m (Fig. 7). The detrital remanence (peaking in cycles with lighter shading) starts to build-up from zero once d_0 has been exceeded. No CRM (peaking in cycles with darker shading) forms at this stage. Below d_2 (at 1.20 m), the CRM also starts to lock-in and the PDRM is locked completely with maximum values of 1. The total remanence signal is constant below d_3 (3.20 m).

Of course, the lock-in function moves progressively upward with ongoing sedimentation. We start out in the reversed field. Hence, at depth, both components are blocked with reversed polarity. When the field reverses, the lock-in function comes into play and determines the proportion of normally and reversely locked remanence components, respectively. Since the pedogenic component is locked later than the detrital component, it acquires an increasingly normal component that is displaced downward (i.e. it occurs apparently earlier than it should). This holds true also for the detrital component at a later stage or nearer the actual reversal boundary. The convolution of the lock-in function with the field behaviour leads to the recording of seven apparent polarity flips. The normal polarity remanence is completely blocked 0.4 m below the end of the field reversal.

An increase in the period of lithogenic ratio $e(z)$ fluctuations will reduce the number of polarity changes. If the period exceeds 0.86 m (as found by trial and error), only a single polarity change will be recorded. Small changes in the PDRM/CRM ratio occurring near a field polarity change can have a strong effect on the modelled NRM polarity pattern. Model calculations show that a 2 cm thick layer with a detrital contribution of 25 per cent at a critical depth in an entirely pedogenic lithology may create an additional apparent polarity zone.

4.1.3 Model for the Lingtai MBB

Eq. (4.3) describes the lock-in process over the whole model space. The lock-in process at the present surface is not of interest for modelling the MBB at Lingtai. Thus, we can transform e.g. (4.3) into:

$$\mathbf{M}(z) = \lambda_{\mathrm{PDRM+CRM}}(z, e(z)) + \int_{\zeta=0}^{z} \lambda_{\mathrm{PDRM+CRM}}(\zeta, e(z))\, \frac{\partial \mathbf{H}(z-\zeta)}{\partial \zeta}\, d\zeta. \tag{4.6}$$

The first term of (4.6) describes the lock-in process at the model surface when $\zeta = z$. As this term is not convolved with the magnetic field, it is identical to the lock-in function. The second term represents the convolution of the lock-in function with the derivative of the magnetic field (see Fig. 5). After lock-in depth d_3 has been reached, the modelled remanence is constant at the maximum value (=1), thus eq. (4.6) changes to:

$$\mathbf{M}(z) = 1 + \int_{\zeta=0}^{z} \lambda_{\mathrm{PDRM+CRM}}(\zeta, e(z))\, \frac{\partial \mathbf{H}(z-\zeta)}{\partial \zeta}\, d\zeta. \tag{4.7}$$

The detrital-pedogenic model assumes that: (1) the correct stratigraphic position of the MBB is in the lower part of S7 as discussed above, and (2) the MBB magnetic field change takes place over a depth interval corresponding to ∼5000 yr at Lingtai. The value of 5000 yr for the MBB reversal was chosen as a compromise between the estimated theoretical and observed geomagnetic reversal durations which range between 1000 and 8000 yr (see Merrill & McFadden 1999). Hence, the constants c_1 and c_2 in Eq. (4.4) are taken as 59.75 m and 60.15 m, respectively.

Both remanence acquisition processes (PDRM and CRM) will not necessarily contribute equally to the natural remanence. With respect to this, the NRM and ARM of two end-member samples were compared. The samples originate from the loess horizon L4 (at 30.42 m) which is dominated by the detrital component and the palaeosol S5 (at 40.62 m) which is dominated by the pedogenic component. Using an average sedimentation rate of 7.9 cm kyr^{-1} during the Brunhes chron, ages of 385 ka and 514 ka are obtained for these two depths, respectively. According to Guyodo & Valet (1999), the strength of the geomagnetic field was approximately the same at both these times, within the uncertainties of their determinations.

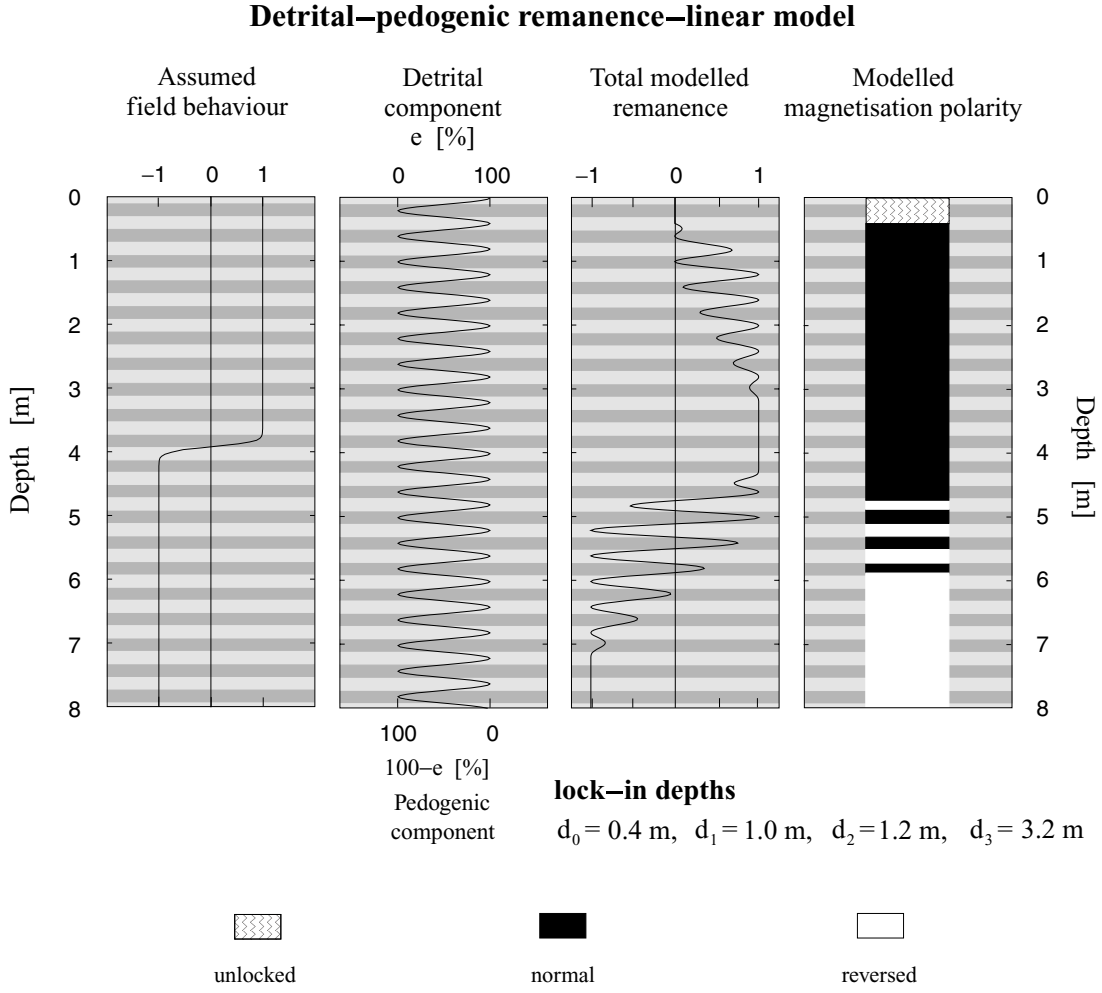

Figure 7. Test of the detrital-pedogenic lock-in model with an artificial lihology. The lithogenic ratio $e(z)$ varies sinusoidally between 0 and 100 per cent every 0.2 m. The modelled detrital-pedogenic remanence changes polarity seven times.

The following ratio can be regarded as an intensity indicator of the characteristic component of the NRM:

$$\frac{\mathrm{NRM}_{20mT} - \mathrm{NRM}_{50mT}}{\mathrm{ARM}_{20mT} - \mathrm{ARM}_{50mT}}. \tag{4.8}$$

The secondary magnetization overprint is usually removed at 20 mT and above 50 mT the NRM becomes unstable (in loess samples). Both detrital and pedogenic components contribute to this magnetization window of the characteristic NRM. If the intensity of the magnetic field is constant, any differences in this ratio are due to different efficiencies of remanence acquisition. The ratio is about (0.174 ± 0.028) in the loess sample and (0.105 ± 0.007) in the palaeosol (see Table 2) which implies that the NRM is more efficiently ($\sim$1.7 times) acquired by PDRM acquisition processes than by CRM acquisition. The lithogenic parameter e has therefore been corrected for NRM acquisition and recalculated:

$$e_{\mathrm{corr}} = \frac{0.174e}{0.174e + 0.105(100 - e)} \cdot 100 \text{ per cent}. \tag{4.9}$$

The variation of the PDRM/CRM ratio $e_{\mathrm{corr}}(z)$ from S7 to S8, as given by ARM measurements e.g. (4.5), has been plotted in Fig. 8. Higher detrital percentages are reached in the upper part of loess L8. The distinct decrease toward the pedogenically pre-dominated palaeosol shows that the ARM signal is much more sensitive to loess alteration than the magnetic parameters shown in Fig. 1.

The modelled polarity pattern shows some common and some differing features with the observed NRM polarity (Fig. 8a). Three polarity changes occur in L8 between 60.86 and 61.26 m. This is not in agreement with the thermal demagnetization results. Hence, the initially assumed lock-in depths have been slightly modified to improve agreement with the observed data. The best-fitting lock-in depths are $d_0 = 0.4$ m, $d_1 = 1.60$ m, $d_2 = 1.70$ m and $d_3 = 3.2$ m (Fig. 8b). After model recalculation, seven polarity changes between 61.48 m and 61.80 m occur. Now, the difference between the midpoints of both multiple magnetization polarity intervals is only 0.03 m.

4.2 The exponential detrital-pedogenic lock-in model

The linear lock-in model is a first-order approximation for remanence acquisition processes on the CLP. Several authors have suggested that exponential lock-in rates may be much closer to reality (Verosub 1977; Hamano 1980; Denham & Chave 1982). In the following, an attempt is made to consider some physical processes for the lock-in process in order to approach a more realistic model.

The PDRM lock-in process in loess is mainly controlled by the pore size p. At shallow depth, the pore size is large enough to allow rotational movement of magnetic particles (or of those to which they are attached). The overburden due to continuing sedimentation causes linearly increasing pressure and reduced pore size with

Table 2. Variability of the ChRM intensity indicator (eq. 4.9).

Demagnetizing AF field [mT]		NRM		ARM		ΔNRM/ΔARM
		20	50	20	50	
Loess L4	~385 ka					
depth [m]	sample					
30.36	A1518	7.13E-05	4.68E-05	2.54E-04	8.49E-05	0.145
30.38	A1519	6.11E-05	3.82E-05	1.99E-04	6.61E-05	0.172
30.42	A1521	7.00E-05	4.47E-05	2.28E-04	5.96E-05	0.150
30.44	A1522	9.14E-05	6.00E-05	2.40E-04	7.95E-05	0.196
30.46	A1523	8.61E-05	5.63E-05	2.11E-04	6.83E-05	0.209
					Mean	0.174
					Standard deviation	0.028
					Rel. standard deviation	16.0
Palaeosol S5	~514 ka					
depth [m]	sample					
40.56	A2028	3.42E-04	8.16E-05	2.71E-03	1.94E-04	0.103
40.58	A2029	3.98E-04	8.99E-05	2.99E-03	1.83E-04	0.110
40.62	A2031	2.76E-04	6.30E-05	2.09E-03	1.56E-04	0.110
40.64	A2032	2.69E-04	6.82E-05	2.30E-03	1.52E-04	0.093
40.70	A2035	3.87E-04	9.37E-05	2.92E-03	2.19E-04	0.109
					Mean	0.105
					Standard deviation	0.007
					Rel. standard deviation	6.7

The samples originate from the most pristine loess L4 and well the developed palaeosol S5, both from Lingtai. The magnetic units are given in Am^2. The peak AF for the acquired ARM was 150 mT and the bias field 0.05 mT.

depth. Hamano (1980) used the void ratio (=volume of air and liquids/volume of solids) as a measure of pressure increasing with depth. In Chinese loess, the void ratio decreases due to compression of the pores, but grain size remains constant (Suzuki & Matsukura 1992). Therefore, the relationship given by Hamano (1980) may be generalized by the following function. The mean pore size $\mu_d(\zeta)$ decreases with increasing burial depth ζ:

$$\mu_d(\zeta) = p_t + (p_i - p_t) \cdot e^{-c_d \zeta}, \tag{4.10}$$

where c_d is a constant (the subscript d referring to the detrital process). p_i and p_t represent initial and terminal pore size, respectively. With increasing burial, the fraction of physically blocked moments is then:

$$\lambda_{\mathrm{PDRM}}(\zeta) = \int_0^{p_b} \frac{1}{\sigma_d \sqrt{2\pi}\, p} e^{-\frac{(\ln p - \mu_d(\zeta))^2}{2\sigma_d^2}} dp. \tag{4.11}$$

A log-normal pore size distribution moves through the critical pore size p_b at which the particles are mechanically fixed. σ_d denotes the standard deviation. Our model calculations use values for p_i and p_t from pore size distributions of sandy Malan loess given by Suzuki & Matsukura (1992). The pore size histogram of this loess exhibits two peaks, at 10 μm and 0.05 μm. The unknown parameters of blocking pore size p_b, constant c_d and σ_d were chosen in such a manner that the detrital lock-in function starts to significantly deviate from zero at about 0.4 m and to reach its maximum at around 1.60 m as discussed above. In this way, values of 0.5 μm for p_b, 3.4 for c_d and 0.6 for σ_d were obtained (Fig. 9).

The CRM acquisition process strongly depends on the volume of the remanence carriers. Grains below the blocking volume V_b cannot retain a remanent magnetization. At the initial stage of pedogenesis, a log-normal distribution of newly forming magnetic grains has its mean $\mu_p(\zeta)$ at V_0, well below V_b. With ongoing time the magnetic particles grow. The distribution crosses V_b and the CRM becomes blocked. We assume that the process of crystallization obeys the same mathematical rules as its reverse process, dissolution. The curve of surface dissolution of goethite, for instance, has a sigmoidal shape (Stucki *et al.* 1988) due to limitation of the dissolution rate. This approach is comparable to surface-controlled chemical processes (Cornell & Schwertmann 1996; van Oorschot 2001). Thus, the volume change per unit time is assumed to be proportional to the volume V. It is further assumed that the concentration of iron ions in the fluid phase of the soil decreases with increasing crystallization. This fixes the limit of the crystallization process described by the term $(1 - \frac{V}{V_e})$ with V_e denoting the end volume:

$$\frac{dV}{dt} = cV\left(1 - \frac{V}{V_e}\right). \tag{4.12}$$

The process starts at time t_0 with an initial volume V_0: $V(t_0) = V_0$. The solution of the differential equation is then (Fig. 10c):

$$V(t) = \frac{V_e}{1 + \left(\frac{V_e}{V_0} - 1\right) e^{c_p t_0 + c_p t}}, \tag{4.13}$$

with the constant c_p representing the (unknown) growth rate. Two problems arise with Eq. (4.13). First, there is no useful information about the time dependence of the crystallization processes of magnetite in soils. Second, our calculations are performed in the depth domain and not in time. Therefore, we arbitrarily adapt equation (4.13) to the burial depth ζ:

$$V(\zeta) = \frac{V_e}{1 + \left(\frac{V_e}{V_0} - 1\right) e^{c_p \zeta_0 + c_p \zeta}}. \tag{4.14}$$

Starting out from a nucleation grain volume of $V_0 = 1 \times 10^{-25}$ m^3 (at depth ζ_0), the grain growth is arbitrarily assumed not to exceed the pseudo-single domain range (PSD) and, hence, the grain diameter will not exceed 0.09 μm ($V_e = 3.82 \times 10^{-22}$ m^3). According to Moon & Merrill (1985), this is the upper limit for single domain magnetite. If a magnetic grain exceeds the stable single domain (SSD) size, the particle contains more than one domain and the magnetization markedly decreases (Fig. 10a). The SSD grain size has been estimated for magnetite to lie between 0.05 to 0.06 μm,

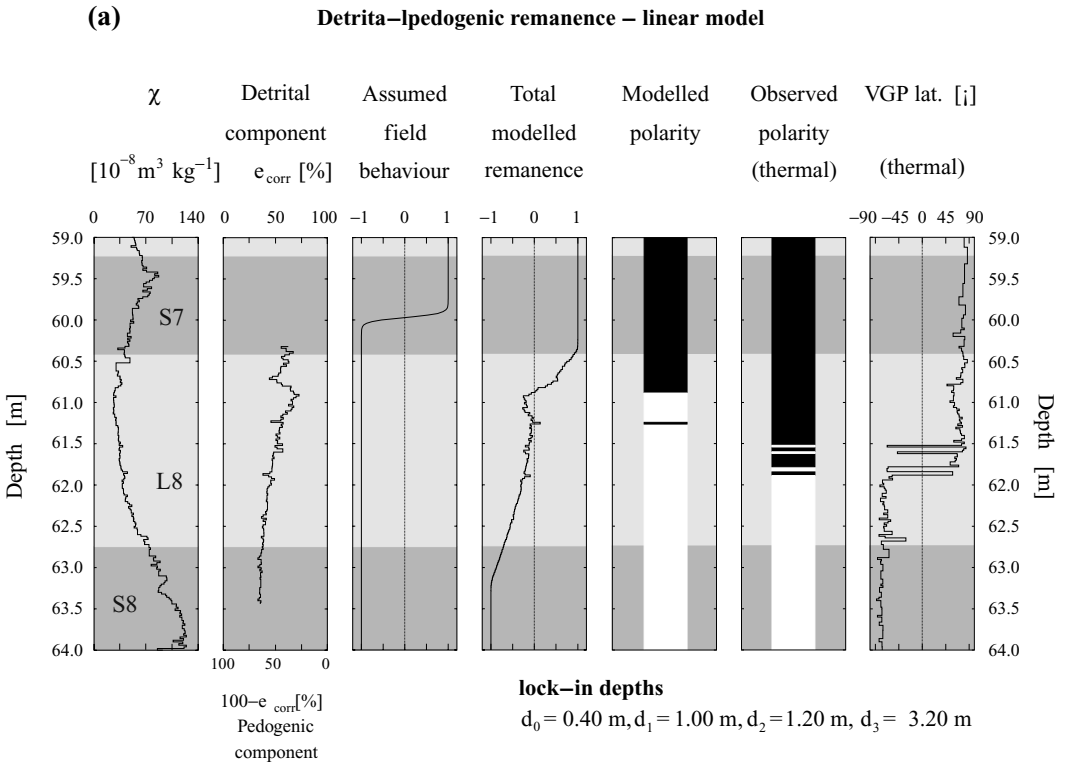

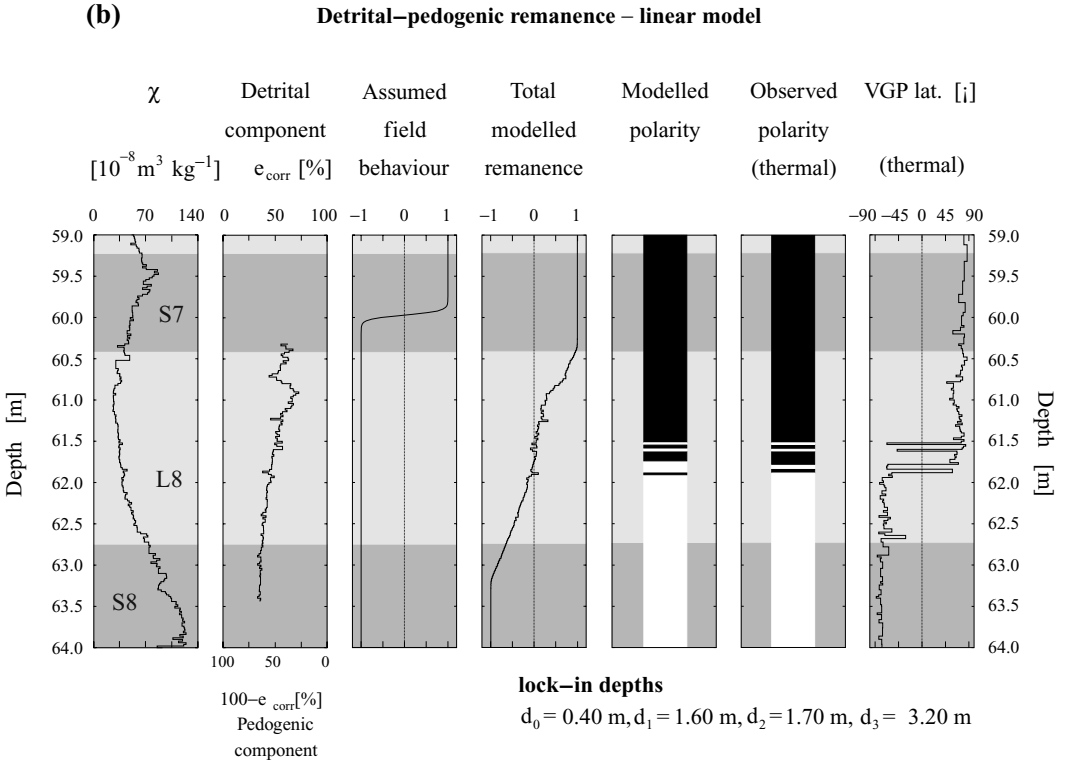

Figure 8. The detrital-pedogenic linear model applied to the loess/palaeosol sediments at Lingtai (central CLP). The changing pedogenic and detrital components cause multiple polarity changes in the modelled remanence. The resolution of the model is 0.02 m. (a) The assumed lock-in depths (see text) do not lead to a good coherence between observed and modelled magnetization polarity flips. (b) Small changes of the lock-in depths lead to an improved agreement with the observed data. The lock-in depths imply nearly equal lock-in rates for the detrital and pedogenic lock-in process. Note that the lithogenic ratio e_{corr} in loess and palaeosol never accomplishes the values of the 'pure' end-members.

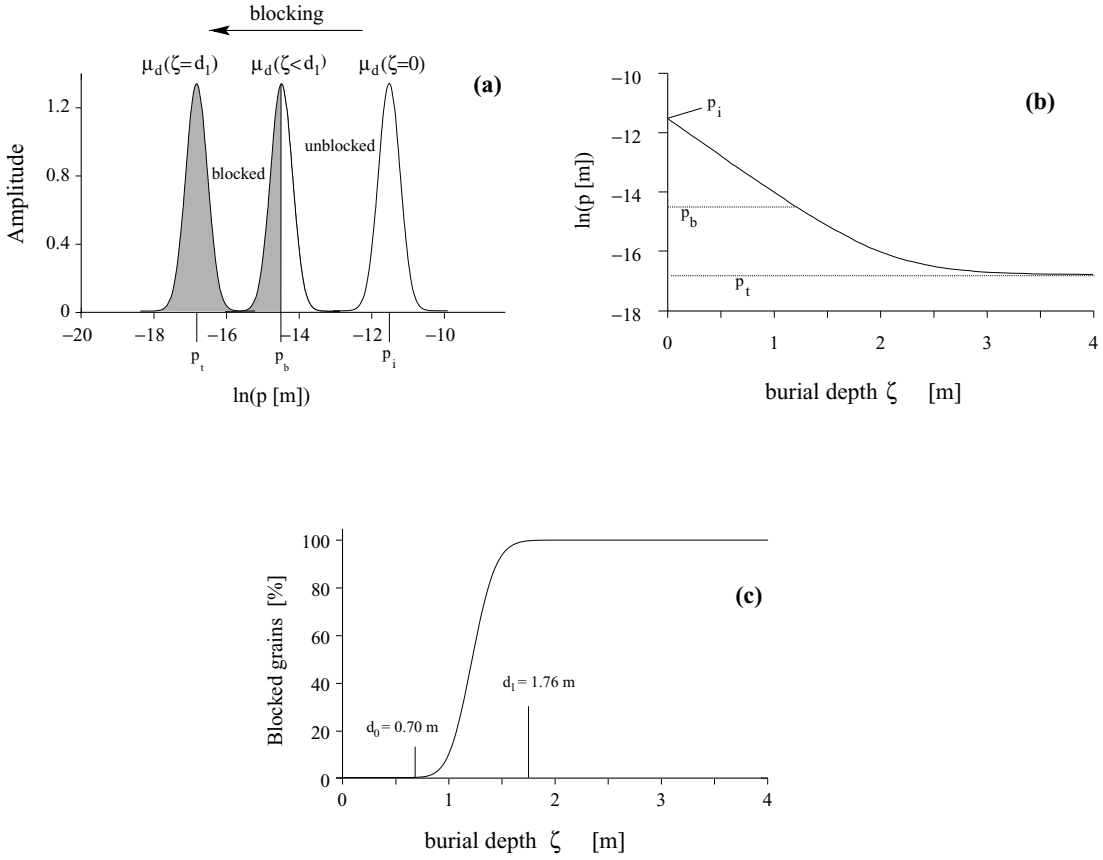

Figure 9. (a) Log-normal distribution of pore sizes. Below a certain pore size, the grains are mechanically fixed and the magnetization is blocked (left, shaded area). (b) Mean of the distribution as a function of burial depth; initial value: p_i. Below a certain depth, the terminal pore size p_t is reached. (c) The percentage of blocked grains calculated by integration from 0 to the blocking pore size p_b. The detrital remanence starts blocking at $d_0 = 0.70$ m and is locked at $d_1 = 1.76$ m. (The lock-in depths correspond to the best-parameters of the exponential model, see Fig. 11b.)

which corresponds to a volume of $V_{\mathrm{SSD}} \approx 1.13 \times 10^{-22}$ m^3 (Dunlop 1973; Argyle & Dunlop 1984).

The grain size dependence of the magnetization has to be taken into account for the blocking of pedogenic grains. ARM versus grain size data (Dunlop & Xu 1993; Egli & Lowrie 2002) have been translated into volumetric data (assuming spherical shape) and fitted with power-law functions (Fig. 10a). The resulting function acts as a weighting factor for the pedogenic lock-in process:

$$\chi_{\mathrm{ARM}}(V) = \begin{cases} 10^{11.5565} \cdot \left(\dfrac{6V}{\pi}\right)^{\frac{1.931}{3}} & V < V_{\mathrm{SSD}} \\ 10^{-5.6689} \cdot \left(\dfrac{6V}{\pi}\right)^{\frac{-0.455}{3}} & V > V_{\mathrm{SSD}}. \end{cases} \tag{4.15}$$

By analogy with Eq. (4.11) the proportion of pedogenically blocked grains (parameters with subscript p) is given by (Fig. 10d):

$$\lambda_{\mathrm{CRM}}(\zeta) = \int_{V_b}^{\infty} \chi_{\mathrm{ARM}}(V) \cdot \frac{1}{\sigma_p \sqrt{2\pi V}} e^{-\frac{(\ln V - \mu_p(\zeta))^2}{2\sigma_p^2}} dV. \tag{4.16}$$

The blocking volume V_b is assumed to be 8.18×10^{-24} m^3. This value implies a grain size of 0.025 μm, which is the lower limit grain size for SD magnetite (McNab *et al.* 1968).

Since sedimentation continues during interglacial stages on the central CLP, burial depth is related to deposition time. Volume growth as a function of increasing burial is shown in Fig. 10(c). The unknown parameters σ_p, c_p, ζ_0 were adapted in order to fix the pedogenic lock-in function (Fig. 10d) between the best-fitting lock-in depths d_2 and d_3 derived from the linear model (*cf.* Fig. 8b).

Calculating the remanence with this non-linear lock-in function leads to more multiple polarity flips (Fig. 11a) compared to the linear model (Fig. 8b). The non-linear lock-in model, however, does not fit the observed data particularly well and significantly deviates from the best fit of the linear model (Fig. 8b). Changing c_d, σ_d, c_p, and ζ_0 to 2.55, 0.4, 5.75 m^2 and 1.12 m, respectively, yields best-fit lock-in depths of $d_0 = 0.7$ m, $d_1 = 1.76$ m, $d_2 = 1.82$ m and $d_3 = 3.2$ m. The results of the exponential lock-in model now become similar to the linear model (Fig. 11b).

These lock-in depths differ considerably from those initially assumed. In view of their uncertainty, it is not worthwhile discussing their accuracy. The linear and the exponential lock-in models both show that small variations of the lithogenic properties can affect the polarity of the magnetization during a reversal. As pedogenic action on the moist central CLP can start as soon as the loess is deposited, the exponential model may be more realistic.

5 DISCUSSION AND CONCLUSIONS

Loess is mechanically unstable after deposition. Below a certain depth, it compacts into a more rigid sediment as the transformation of dust into loess, coupled with secondary calcification, builds up a

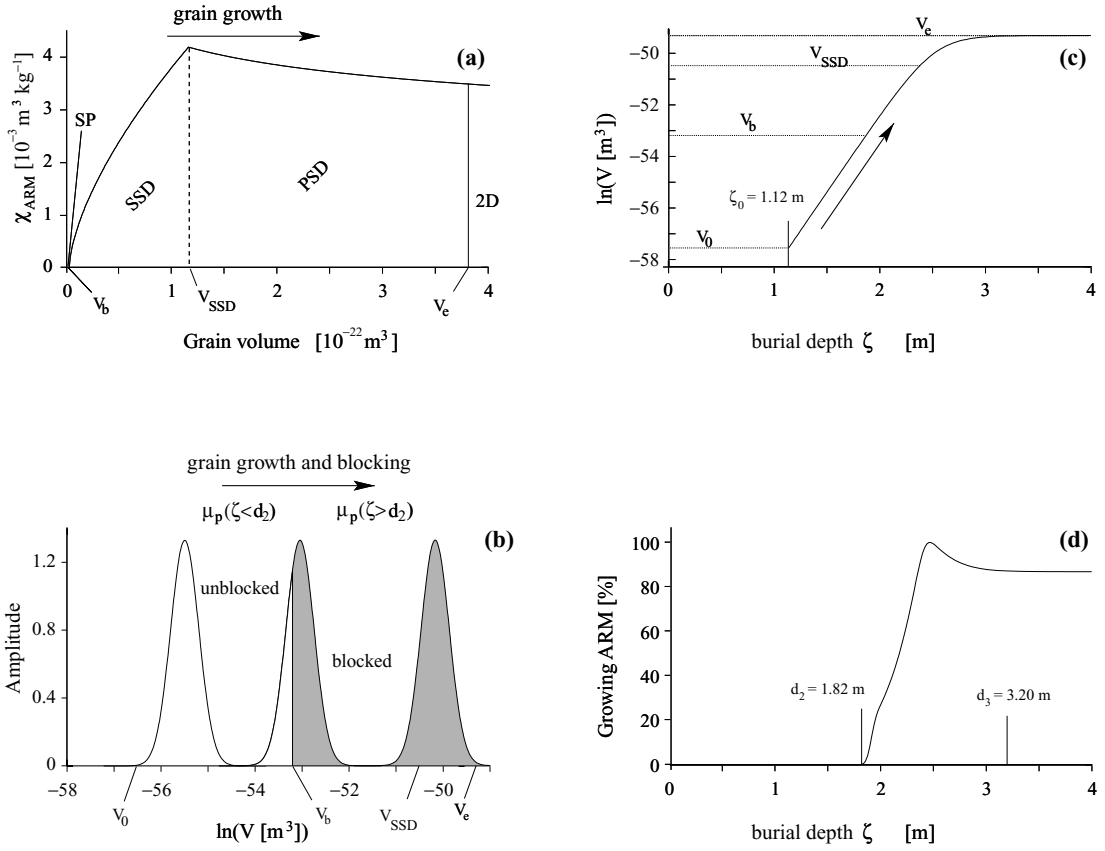

Figure 10. (a) ARM susceptibility (χ_{ARM}) of magnetite as a function of grain volume. χ_{ARM} increases within the single domain range. Above 1.13×10^{-22} m^3 (0.06 μm diameter) the pseudo-single domain stage (PSD) is reached and χ_{ARM} slowly decreases. (b) Magnetic grains below V_b cannot retain a remanent magnetization (left), and are not blocked. A log-normal distribution of chemically formed grains grows through the blocking volume V_b (arrow). The blocked grains reach the end volume $V = V_e$. (c) Assumed mean magnetite grain volumes with increasing burial depth. Grain growth stops below a certain depth and the grains reach their final two-domain (2-D) volume of 3.82×10^{-22} m^3 (diameter = 0.09 μm). (d) The growing ARM is represented by the integral of the distribution multiplied with χ_{ARM} between V_b and infinity. Because of the decrease of χ_{ARM} above 1.13×10^{-22} m^3, the contribution at large ζ is less than at the maximal value V_{SSD} and is taken as the characteristic value for the equivalent CRM. The lock-in depths and ζ_0 correspond to the best-fitting parameters of the exponential model (Fig. 11b). In this model, grain growth starts at $\zeta_0 = 1.12$ m and CRM blocking begins at $d_2 = 1.82$ m. The lock-in process is completed at $d_3 = 3.20$ m.

microstructure. This structural change takes place between ∼0.4 and ∼1 m under specific loading and wetting conditions (Assallay *et al.* 1998), and, among other things, leads to the mechanical fixing of the magnetic grains. Our linear modelling results for the Lingtai section support the idea that the post-depositional remanent magnetization is blocked over approximately this depth zone.

Under sufficiently moist and warm climate conditions, chemical weathering releases iron ions as a basis for the formation of secondary pedogenic iron minerals. Evans & Heller (1994) proposed the coexistence of two magnetic mineral components in loess/palaeosol sediments on the CLP: the primary component is a detrital assemblage of magnetic particles, which appears to be uniform across the entire loess plateau. The second component is an authigenic phase varying between sites and also from layer to layer in a section. The measurements and modelling presented here confirm this suggestion: a low coercivity mineral component (P) is enriched with increasing degree of pedogenesis, whereas the detrital component (D) remains rather constant.

Mineral-magnetic analysis suggests that post-depositional and (bio-) chemical recording processes occur at different stages of burial and therefore at different moments in time and in geomagnetic field history. The relative contribution of the two recording mechanisms has been estimated on the basis of differences in the ARM coercivity spectra. The two lock-in models considered in this paper take both, PDRM and CRM acquisition into account. Piecewise linear lock-in functions lead to a reasonable agreement with the observed data. The exponential model, which seems to be more relevant physically, yields essentially the same results.

Considering that low values and variations of the modelled remanence intensities allow for multiple polarity flips, one could argue that these signal variations are simply random noise. However, the occurrence of a low magnetization intensity zone is an important property of the two component lock-in model if detrital and authigenic carriers contribute at nearly equal proportions (see zero remanence plateau of the 50 per cent PDRM/CRM curve in Fig. 5). Consequently, minor lithogenic variations can easily cause multiple polarity flips, which by no means are caused by rapid geomagnetic field changes. Although the intensity of the magnetic field may also be reduced, the low magnetization zone is mostly due to the lithogenic properties of the sediment and the secondary formation of magnetic minerals. The actual data at Lingtai also exhibit such a zone of low NRM intensity during the MBB transition (Spassov *et al.* 2001).

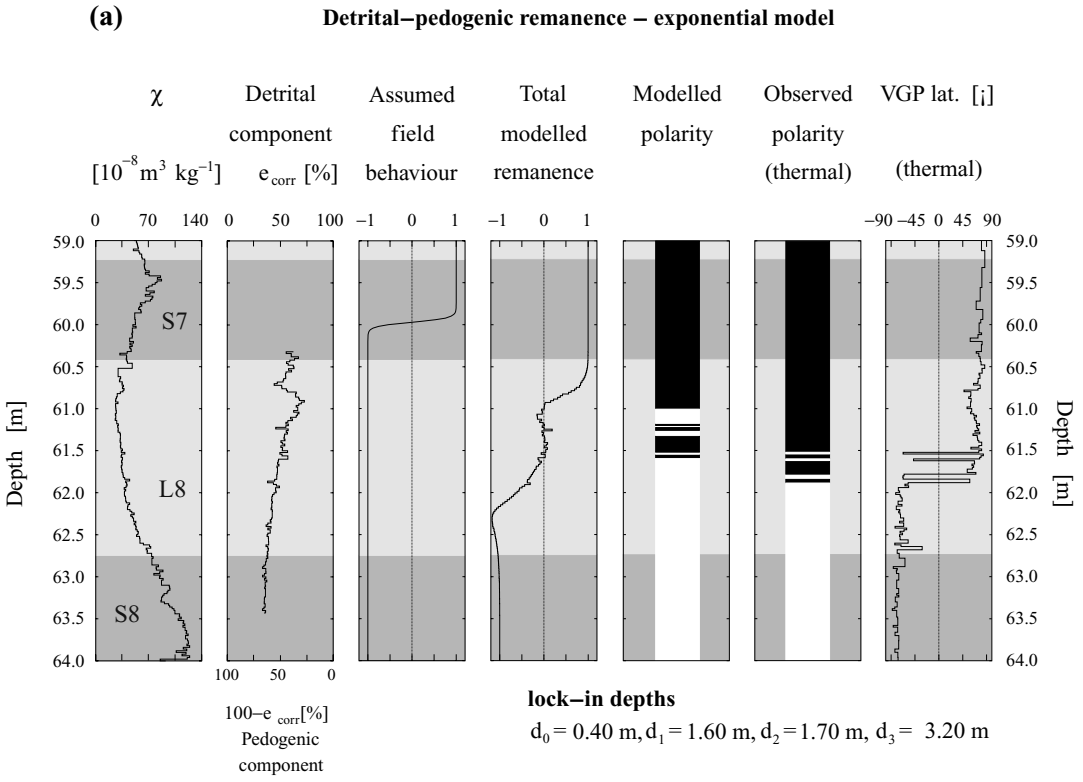

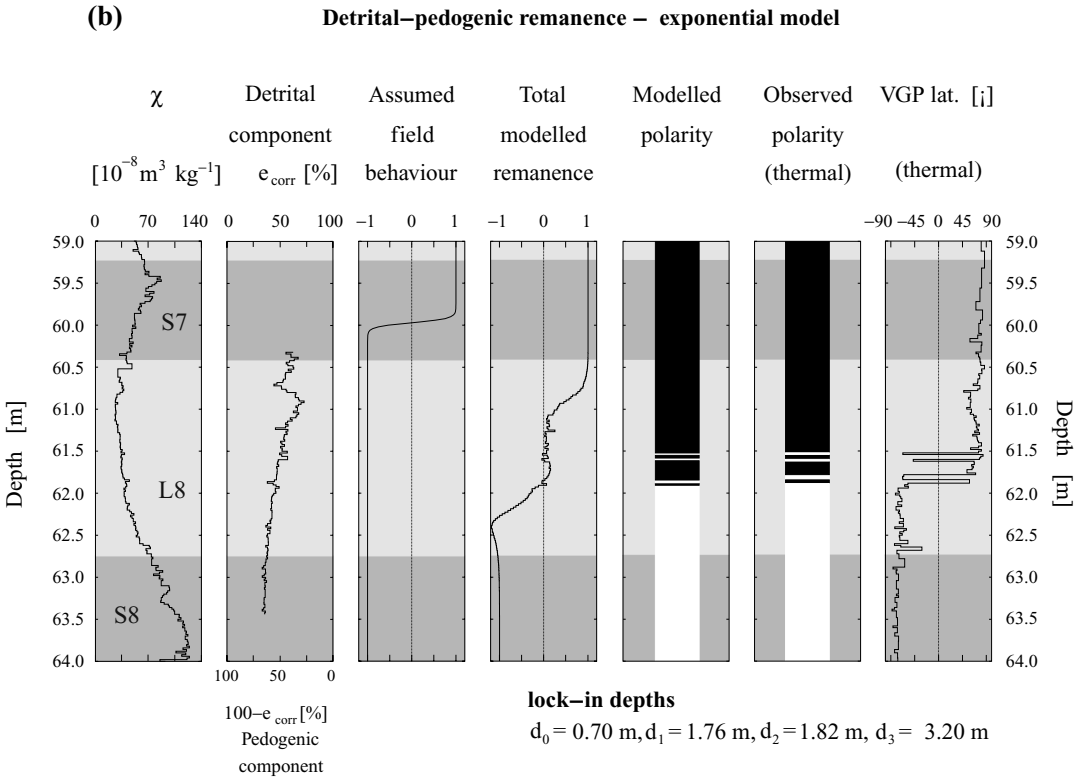

Figure 11. Exponential detrital-pedogenic lock-in model for the loess-palaeosol sediments around the MBB at Lingtai. This model also produces multiple polarity changes. (a) The resulting model zonation differs substantially from the observed polarity pattern and is offset by about 0.5 m when using the optimal lock-in depths of the linear model for the parameter estimation (see text). (b) Optimized parameters lead to different lock-in depths and high similarity between model and observation.

A general problem of lock-in processes is the incorporation of depth and time dependent processes. The fixing of magnetic grains in loose sediments depends mainly on the pore size, which decreases with increasing pressure resulting from increasing burial. Therefore the depositional lock-in process depends on burial depth and not on burial time (Bleil & von Dobeneck 1999). The change of the Earth's magnetic field on the other hand depends on time, not on burial. Thus the calculated magnetization is a function of both time and depth. Several authors simplify the calculations and perform model calculations in only the depth domain (Bleil & von Dobeneck 1999; Hyodo 1984). Calculations in the depth domain are legitimate only for depositional lock-in processes because the transformation from time to depth is linear. This may be not the case for CRM acquisition. The CRM lock-in process depends strongly on the grain volume, which is supposed to increase with time. The burial dependence is indirectly incorporated by assuming ongoing sedimentation of loess during soil development, which is the case in areas of high dust accumulation such as the CLP. Sediment accumulation during soil development and, thus, the indirect burial dependence of CRM acquisition is not well known.

With these precautions in mind, the following conclusions can be drawn from modelling the NRM lock-in process at Lingtai.

The linear detrital-pedogenic remanence model is able to explain the downward shift of the MBB in the loess/palaeosol sequence at Lingtai on the central CLP. A displacement from the stratigraphic expected level of 1.74 m (corresponding to a time delay of about 22 kyr) results from the model considerations. The model further explains the observed occurrence of multiple polarity changes by small variations of closely balanced contributions of the detrital and pedogenic mineral components during the MBB polarity change. The good agreement of the modelled results with the observed data supports the hypothesis of two remanence acquisition processes to be involved in the loess sediments of the central CLP: post-depositional (PDRM) and chemical (CRM) remanent magnetization.

The observed multiple polarity changes of the ChRM component are not features of the geomagnetic field during the MBB. They are caused by variable relative contributions of detrital and pedogenic magnetization components during the reversal, which give rise to irregular polarity lock-in at the MBB. Hence, virtual geomagnetic pole paths during reversals from profiles of the central CLP are not representative of geomagnetic field behaviour.

The actual physical deposition processes are most probably not of a simple linear nature. Therefore an attempt has been made to explain the displaced and complicated MBB by a non-linear lock-in model. This model also explains the downward shift of the MBB and the multiple polarity changes. It is in better agreement with the observations than the linear model. Further fundamental data such as blocking pore size, rate of pedogenic grain growth and lock-in depths are needed to obtain better information about the model parameters. The acquisition process of the NRM also needs to be studied. In addition, the simplistic function of the geomagnetic field during the M/B reversal may be replaced with more realistic data for the Earth's magnetic field as given for instance by the SINT800 palaeointensity stack (Guyodo & Valet 1999) or by reversal simulations (Coe *et al.* 2000).

The recognition of a delayed Matuyama-Brunhes boundary in loess/palaeosol sequences on the Chinese Loess Plateau solves their conflict with palaeoclimatic records from the marine realm. Hence the Chinese palaeosol S7 almost certainly corresponds to the marine oxygen isotope stage 19, as postulated by Heller *et al.* (1987), Zhou & Shackleton (1999) and Heslop *et al.* (2000).

The linear detrital-pedogenic lock-in model is proposed as a first step in solving delayed remanence acquisition processes in sediments with complex recording histories. It yields promising results in the loess/palaeosol sequences of the central CLP. The model can be tested using other well-defined reversal boundaries and other loess lithologies, for instance, on the western CLP. Further experiments concerning the dynamics of CRM acquisition have to be performed to improve mathematical simulations.

Bleil & von Dobeneck (1999) already demonstrated for marine sediments that pseudo-records of palaeointensities can be obtained just by varying the lithology at low to intermediate sedimentation rates (1–4 cm kyr^{-1}). On the central CLP, two or more magnetic mineral populations with variable relative contributions almost always coexist. Their complex interaction and blocking will hamper or even prohibit useful information on palaeointensity changes, palaeosecular variation and polarity transition features during major reversals and/or excursions.

ACKNOWLEDGMENTS

We thank Ramon Egli for his constructive discussions and encouraging comments. Special thanks go to David Heslop and Andrew Roberts for a careful review of the manuscript. This study was financed by Swiss National Science foundation grant No 21-54143.98.

REFERENCES

Argyle, K.S. & Dunlop, D.J., 1984. Theoretical domain structure in multidomain magnetite particles, *Geophys. Res. Lett.,* **11,** 185–188.

Assallay, A.M., Jefferson, I., Rogers, C.D.F. & Smalley, I.J., 1998. Fragipan formation in loess soils: development of the Bryant hydroconsolidation hypothesis, *Geoderma,* **83,** 1–16.

Bleil, U. & von Dobeneck, T., 1999. Geomagnetic events and relative palaeointensity records—clues to high-resolution palaeomagnetic chronostratigraphies of Late Quaternary marine sediments?, in *Use of Proxies in Paleoceanography: Examples from the South Atlantic,* pp. 635–654, eds Fischer, G. & Wefer, G., Springer-Verlag, Berlin, Heidelberg.

Cao, J.X., Xu, Q.Z., Zhang, Y.T. & Cheng, F.F., 1988. Investigation on loess-palaeosol in Jiuzhoutai, Lanzhou and its environmental evolution, *Journal of Lanzhou University,* **24,** 118–122.

Carter-Stiglitz, B., Moskowitz, B. & Jackson, M., 2001. Unmixing magnetic assemblages and the magnetic behaviour of bimodal mixtures, *J. geophys. Res.,* **106,** 26 397–26 411.

Cisowski, S., 1981. Interacting vs. non-interacting single-domain behavior in natural and synthetic samples, *Phys. Earth planet. Inter.,* **26,** 77–83.

Coe, R.S., Hongre, L. & Glatzmaier, G.A., 2000. An examination of simulated geomagnetic reversals from a paleomagnetic perspective, *Phil. Trans. R. Soc. Lond.,* A, **358,** 1141–1170.

Cornell, R.M. & Schwertmann, U., 1996. *The Iron Oxides,* VCH Publishers, Weinheim, New York, Basel, Cambridge, pp. 1–573.

deMenocal, P., Ruddiman, F. & Kent, D.V., 1990. Depth of post-depositional remanence acquisition in deep-sea sediments: a case study of the Brunhes-Matuyama reversal and oxygen isotope stage 19.1, *Earth planet. Sci. Lett.,* **99,** 1–13.

Denham, C.R. & Chave, A.D., 1982. Detrital remanent magnetization: viscosity theory of the lock-in zone, *J. geophys. Res.,* **87,** 7126–7130.

Ding, Z.L., Sun, J.M., Yang, S.L. & Liu, T.S., 1998. Preliminary magnetostratigraphy of a thick aeolian red clay-loess sequence at Lingtai, the Chinese Loess Plateau, *Geophys. Res. Lett.,* **25,** 1225–1228.

Dunlop, D.J., 1973. Superparamagnetic and single-domain threshold sizes in magnetite, *J. geophys. Res.,* **78,** 1780–1793.

Dunlop, D.J. & Özdemir, Ö., 1997. *Rock Magnetism, Fundamentals and Frontiers,* Cambridge University Press, Cambridge, New York, Melbourne, pp. 1–573.

Dunlop, D.J. & Xu, S., 1993. A comparison of methods of granulometry and domain structure determination (abstract), *EOS, Trans. Am. geophys. Un.,* **74,** Fall Meeting suppl., 203.

Egli, R., 2003. Analysis of the field dependence of remanent magnetization curves, *J. geophys. Res.,* **108,** 2081, doi 10.1029/2002JB002023.

Egli, R. & Lowrie, W., 2002. Anhysteretic remanent magnetization of fine magnetic particles, *J. geophys. Res.,* **107,** 2209, doi 10.1029/2001JB000671.

Evans, M.E. & Heller, F., 1994. Magnetic enhancement and palaeoclimate: study of a loess/palaeosol couplet across the loess plateau of China, *Geophys. J. Int.,* **117,** 257–264.

Evans, M.E. & Heller, F., 2001. Magnetism of loess/palaeosol sequences: recent developments, *Earth Science Reviews,* **54,** 129–144.

Eyre, J.K., 1996. The application of high resolution IRM acquisition to the discrimination of remanence carriers in Chinese loess, *Studia geophysica et geodetica,* **40,** 234–242.

Fabian, K. & von Dobeneck, T., 1997. Isothermal magnetization of samples with stable Preisach function: A survey of hysteresis, remanence and rock magnetic parameters, *J. geophys. Res.,* **102,** 17 659–17 677.

Guinasso, N.L. & Schink, D.R., 1975. Quantitative estimates of biological mixing rates in abyssal sediments, *J. geophys. Res.,* **80,** 3032–3043.

Guyodo, Y. & Valet, J.-P., 1999. Global changes in intensity of the Earth's magnetic field during the past 800 kyr, *Nature,* **399,** 249–252.

Hamano, Y., 1980. An experiment on the post-depositional remanent magnetization in artificial and natural sediments, *Earth planet. Sci. Lett.,* **51,** 221–232.

Heller, F. & Liu, T.S., 1982. Magnetostratigraphical dating of loess deposits in China, *Nature,* **300,** 431–433.

Heller, F. & Liu, T.S., 1984. Magnetism of Chinese loess deposits, *Geophys. J. R. astr. Soc.,* **77,** 125–141.

Heller, F., Meili, B., Wang, J.D., Li, H.M. & Liu, T.S., 1987. Magnetization and sedimentation history of loess in the central loess plateau of China, in *Aspects of Loess Research,* pp. 147–163, ed. Liu, T.S., China Ocean Press, Beijing.

Heslop, D., Langereis, C.G. & Dekkers, M.J., 2000. A new astronomical timescale for the loess deposits of Northern China, *Earth planet. Sci. Lett.,* **184,** 125–139.

Hus, J.J. & Han, J., 1992. The contribution of loess magnetism in China to the retrieval of past global changes—some problems, *Phys. Earth planet. Inter.,* **70,** 154–168.

Hyodo, M., 1984. Possibility of reconstruction of the past geomagnetic field from homogeneouments, *J. Geomag. Geoelectr.,* **36,** 45–62.

Irving, E. & Major, A., 1964. Post-depositional detrital remanent magnetization in a synthetic sediment, *Sedimentology,* **3,** 135–143.

Kent, D.V., 1973. Post depositional remanent magnetization in deep sea sediments, *Nature,* **246,** 32–34.

Kent, D.V. & Schneider, D.A., 1995. Correlation of paleointensity variation records in the Brunhes/Matuyama geomagnetic polarity transition interval, *Earth planet. Sci. Lett.,* **129,** 135–144.

Kneller, E.F. & Luborsky, F.E., 1963. Particle size dependence of coercivity and remanence of single-domain particles, *J. appl. Phys.,* **34,** 656–658.

Kruiver, P.P., Dekkers, M.J. & Heslop, D., 2001. Quantification of magnetic coercivity components by the analysis of acquisition curves of isothermal remanent magnetisation, *Earth planet. Sci. Lett.,* **189,** 269–276.

Li, C.L., Ouyang, Z.Y., Liu, T.S. & An, Z.S., 1993. Microtektites and glassy microspherules in loess—their discoveries and implications, *Science in China,* 1141–1152.

Li, J.J. *et al.,* 1997. Magnetostratigraphic dating of river terraces: Rapid and intermittent incision by the Yellow River of the northeastern margin of the Tibetan Plateau during Quaternary, *J. geophys. Res.,* **102,** 10 121–10 132.

Liu, T.S, 1985. *Loess and the Environment,* China Ocean Press, Beijing, pp. 1–251.

Liu, T.S. & Chang, T.H., 1964. The 'Huangtu' (Loess) of China, *Report of the VIth International congress of Quaternary, Warsaw, 1961, IV: Symposium on Loess,* ódź.

Liu, X.M., Liu, T.S., Xu, T.C., Liu, C. & Chen, M.Y., 1988. The Chinese loess in Xifeng I. The primary study on magnetostratigraphy of a loess profile in Xifeng area, Gansu province, *Geophys. J.,* **92,** 345–348.

Løvlie, R., 1974. Post-depositional remanent magnetization in a redeposited deep-sea sediment, *Earth planet. Sci. Lett.,* **21,** 315–320.

Løvlie, R., 1976. The intensity pattern of post-depositional remanence acquired in some sediments during a reversal of the external magnetic field, *Earth planet. Sci. Lett.,* **30,** 209–214.

Maher, B.A., 1988. Magnetic properties of some synthetic sub-micron magnetites, *Geophys. J.,* **94,** 83–96.

Mazaud, A., 1996. 'Sawtooth' variation in magnetic intensity profiles and delayed acquisition of magnetization in deep sea cores, *Earth planet. Sci. Lett.,* **139,** 57–69.

McNab, T.K., Fox, R.A. & Boyle, A.F.J., 1968. Some magnetic properties of magnetite (Fe_3O_4) microcrystals, *J. appl. Phys.,* **39,** 5703–5711.

Merrill, R.T. & McFadden, P.L., 1999. Geomagnetic polarity transitions, *Review of Geophysics,* **37,** 210–226.

Meynadier, L. & Valet, J.-P., 1996. Post-depositional realignment of magnetic grains and asymmetric saw-tooth patterns of magnetization intensity, *Earth planet. Sci. Lett.,* **140,** 123–132.

Moon, T.S. & Merrill, R.T., 1985. Nucleation theory and domain states in multidomain magnetic material, *Phys. Earth planet. Inter.,* **37,** 214–222.

Niitsuma, N., 1977. Zone-magnetisation model and depth lag of NRM in deep-sea sediments, *Rock Magnetism and Paleogeophysics,* **4,** 65–71.

Otofuji, Y. & Sasajima, S., 1981. A magnetization process of sediments: laboratory experiments on post-depositional remanent magnetization, *Geophys. J. R. astr. Soc.,* **66,** 241–259.

Perel'man, A.I., 1977. *Geochemistry of Elements in the Supergene Zone,* Keter, Jerusalem, pp. 1–266.

Roberts, A.P., Cui, Y.-L. & Verosub, K.L., 1995. Wasp-waisted hysteresis loops: mineral magnetic characteristics and discrimination of components in mixed magnetic systems, *J. geophys. Res.,* **100,** 17 909–17 924.

Robertson, D.J. & France, D.E., 1994. Discrimination of remanence-carrying minerals in mixtures, using isothermal remanent magnetisation acquisition curves, *Phys. Earth planet. Inter.,* **82,** 223–234.

Rolph, T.C., Shaw, J., Derbyshire, E. & Wang, J.T., 1989. A detailed geomagnetic record from Chinese loess, *Phys. Earth planet. Inter.,* **56,** 151–164.

Rutter, N., Ding, Z.L., Evans, M.E. & Wang, Y.C., 1990. Magnetostratigraphy of the Baoji Loess-Palaeosol section in the North-Central China Loess Plateau, *Quaternary International,* **7/8,** 97–102.

Rutter, N., Ding, Z.L., Evans, M.E. & Liu, T.S., 1991. Baoji-type pedostratigraphic section, loess plateau, north-central China, *Quaternary Science Reviews,* **10,** 1–22.

Sartori, M., 2000. The Quaternary climate in loess sediments: Evidence from rock and mineral magnetic and geochemical analysis, *PhD thesis,* ETH Zürich, Switzerland.

Schneider, D.A., Kent, D.V. & Mello, G.A., 1992. A detailed chronology of the Australasian impact event, the Brunhes-Matuyama geomagnetic polarity reversal and global climate change, *Earth planet. Sci. Lett.,* **111,** 395–405.

Shackleton, N.J., Berger, A.L. & Peltier, W.R., 1990. An alternate astronomical calibration of the lower Pleistocene timescale based on ODP site 677, *Transactions of the Royal Society Edinburgh, Earth Sciences,* **81,** 251–261.

Spassov, S., Heller, F., Evans, M.E., Yue, L.P. & Ding, Z.L., 2001. The Matuyama/Brunhes geomagnetic polarity transition at Lingtai and Baoji, Chinese loess plateau, *Physics and Chemistry of the Earth (A),* **26,** 899–904.

Spell, T. & McDougall, I., 1992. Revisions to the age of the Brunhes-Matuyama boundary and the Pleistocene geomagnetic polarity time scale, *Geophys. Res. Lett.,* **19,** 1181–1184.

Stacey, F.D., 1963. The physical theory of rock magnetism, *Advances in Physics,* **12,** 45–133.

Stucki, J.W., Goodman, B.A. & Schwertmann, U., 1988. *Iron in Soils and Clay Minerals,* Reidel Publishing, Dordrecht, Boston, Lancaster, Tokyo, pp. 1–893.

Suzuki, T. & Matsukura, Y., 1992. Pore–size distribution of loess from the loess plateau, China, *Transactions of the Japanese Geomorphological Union,* **13-3,** 169–183.

Tauxe, L., Herbert, T., Shackleton, N.J. & Kok, Y.S., 1996. Astrononomical calibration of the Matuyama-Brunhes boundary: consequences for

magnetic remanence acquisition in marine carbonates and Asian loess sequences, *Earth planet. Sci. Lett.,* **140,** 133–146.

van Oorschot, I.H.M., 2001. Chemical distinction between lithogenic and pedogenic iron oxides in environmental magnetism, *PhD thesis,* Universiteit Utrecht, The Netherlands.

Verosub, K.L., 1977. Depositional and postdepositional processes in the magnetization of sediments, *Review of Geophysics and Space Physics,* **15,** 129–143.

Zheng, H.B., An, Z.S. & Shaw, J., 1992. New contributions to Chinese Plio-Pleistocene magnetostratigraphy, *Phys. Earth planet. Inter.,* **70,** 146–153.

Zhou, L.P. & Shackleton, N.J., 1999. Misleading positions of geomagnetic reversal boundaries in Eurasian loess and implications for correlation between continental and marine sediment sequences, *Earth planet. Sci. Lett.,* **168,** 117–130.

Zhu, R.X., Pan, Y.X., Guo, B. & Liu, T.S., 1998. A recording phase lag between ocean and continent climate changes: constrained by the Matuyama/Brunhes polarity boundary, *Chinese Science Bulletin,* **43,** 1593–1598.